J. Fluid Mech. (1989), *vol.* 208, *pp.* 459–478
Printed in Great Britain

Axisymmetric convection at large Rayleigh and infinite Prandtl number

By AKIRA UMEMURA[1] AND F. H. BUSSE[2]

[1] Department of Mechanical Engineering, Yamagata University, Yonezawa 992, Japan
[2] Physikalisches Institut, Universität Bayreuth, 8580 Bayreuth, Germany

(Received 20 September 1988)

A matched-asymptotic analysis has been carried out for an axisymmetric convection cell in the case of stress-free boundaries. This problem differs from that of two-dimensional convection rolls mainly through the special role played by the central plume. The radius, of order ϵ, of the latter depends on the Rayleigh number R through the relationship $\epsilon^4(-\ln\epsilon) = R^{-\frac{2}{3}}$. The plume velocity is independent of height at lowest order and its magnitude exceeds by a factor $(-\ln\epsilon)^{\frac{1}{2}}$ the strength, of order $R^{\frac{2}{3}}$, of the core flow. As a result of these properties the central plume is governed by advection, in contrast to the perimeter plume which is affected by conduction as well. This asymmetry is reflected in the different thickness of the horizontal thermal boundary layers and gives rise to the deviation of the core temperature from the mean value of the top and bottom temperatures. This deviation is positive (negative) for the case of a falling (rising) central plume. While the core flow is driven mainly by the perimeter plume the fraction of the heat flux carried by the central plume is always above three-quarters and increases as the radius-to-height-ratio λ decreases.

1. Introduction

Convection in a layer heated from below has long been studied as a particularly revealing example of nonlinear fluid mechanics. The numerous applications in geophysical and engineering problems have contributed to the interest in high-Rayleigh-number convection, where the heat transport by fluid motion by far exceeds that carried by molecular conduction. Among the theories on high-Rayleigh-number convection, those based on asymptotic boundary-layer methods have played a special role even though the assumptions on which they rely are not always realized in experimentally or geophysically observed systems. In spite of the restricting assumptions the stationary boundary-layer models appear to capture the main physical features governing high-Rayleigh-number convection. There is thus a continuing interest in asymptotic models particularly as the Rayleigh numbers accessible to numerical simulations of convection flows have grown dramatically in the past decade.

Asymptotic analysis and numerical computations complement each other in that the former have elucidated the spatial scales and nonlinear mechanisms seen in the numerical results. The computations, on the other hand, can simulate the time-dependent processes that cannot easily be treated by asymptotic methods. Most of the attention in this area of research has been focused on two-dimensional convection because of the additional complexity of the third dimension. Boundary-layer models of two-dimensional convection in a high-Prandtl-number fluid have been published

by Turcotte & Oxburgh (1967), Robinson (1967), Roberts (1979), Olson & Corcos (1980) and others. By refining the boundary-layer analysis and associated numerical calculations the accuracy of the approximations for the exact asymptotic solution has been improved and reliable results have been obtained in the case of stress-free boundaries. In the present paper the analysis is extended to the case of an axisymmetric convection cell.

Axisymmetric convection is generally regarded as a prototype of the cellular convection cells typically observed in nature and in many experiments. It exhibits the characteristic asymmetry between rising and descending flow found in hexagonal convection cells and it is also closely related to the axisymmetric quadrupolar convection pattern that is found in theories of convection on the Earth's mantle (Busse 1983; Machetel & Rabinowicz 1985; Machetel & Yuen 1988). Because of the asymmetry two different solutions exist, corresponding to the two signs of motion in the centre. As long as the boundary conditions and the material properties satisfy certain symmetry properties with respect to the midplane of the convection cell, both solutions transport the same amount of heat and do not differ in their integral properties. They can actually be transformed into each other by a reflection at the midplane. When material properties such as the viscosity are temperature dependent, one of the two solutions will be preferred in general. In this paper, however, only the symmetric case will be considered.

Characteristic of axisymmetric convection is the flow feature of a central plume, which will be analysed in §3 after the mathematical formulation of the problem has been given in §2. Sections 4 and 5 treat the analysis of the other thermal boundary layers which, together with the matching condition at the corners, leads to the complete system of equations. Discussion of the results is given in §6.

2. Mathematical formulation of the problem

We consider a pill-box shaped convection cell of height d and radius λd with constant temperatures prescribed at top and bottom (see figure 1). All boundaries are assumed stress-free and the cylindrical sidewall is assumed to have a much lower conductivity than the convecting fluid. Using d as a lengthscale, κ/d as a scale of the velocity where κ is the thermal diffusivity, and the applied temperature difference ΔT as a scale of temperature we obtain the following dimensionless equations for the velocity vector $\boldsymbol{V}$ and the excess θ of the temperature over the mean value between the upper and lower boundaries:

$$\boldsymbol{\nabla}\cdot\boldsymbol{V}=0, \tag{2.1a}$$

$$\boldsymbol{\nabla}^2\boldsymbol{V}-\boldsymbol{\nabla}p+R\theta\boldsymbol{i}_z=0, \tag{2.1b}$$

$$\boldsymbol{V}\cdot\boldsymbol{\nabla}\theta=\boldsymbol{\nabla}^2\theta, \tag{2.1c}$$

where $\boldsymbol{i}_z$ is the vertical unit vector and R is the Rayleigh number $R=\gamma g\Delta T d^3/\kappa\nu$ in the familiar definition. Since we are only interested in steady solutions of the problem, the time derivatives have been neglected in (2.1). We have also assumed the limit of infinite Prandtl number, when the kinematic viscosity ν far exceeds the thermal diffusivity, such that the momentum advection terms can always be neglected.

For the description of the solution we shall use a system of cylindrical coordinates

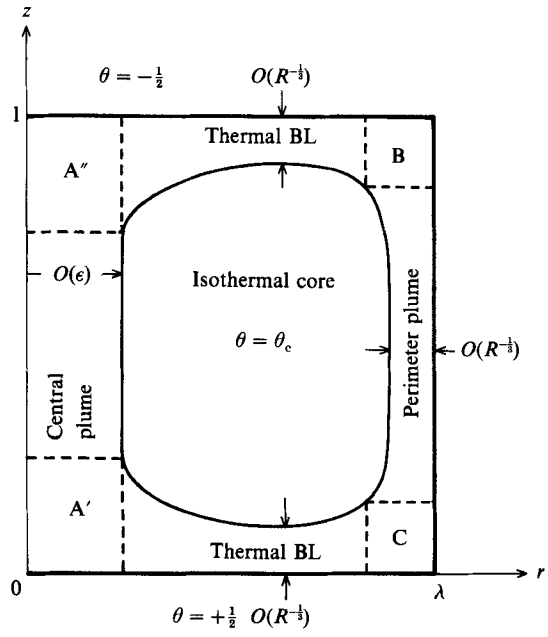

FIGURE 1. Configuration of the problem. The isothermal region which occupies most of the cell interior is surrounded by the central plume A′–A″, top thermal boundary layer A″–B, perimeter plume B–C and bottom thermal boundary layer C–A′ connected at the corners A′, A″, B and C.

(r, z). Restricting attention to the axisymmetric case we introduce the stream function ψ,

$$v_r \equiv u = -\frac{1}{r}\frac{\partial \psi}{\partial z}, \quad v_z \equiv w = \frac{1}{r}\frac{\partial \psi}{\partial r}, \tag{2.2}$$

The boundary condition can now be expressed in the form

$$\psi = \frac{\partial w}{\partial r} = \frac{\partial \theta}{\partial r} = 0 \quad \text{at} \quad r = 0, \lambda, \tag{2.3a}$$

$$\psi = \frac{\partial u}{\partial z} = \theta \pm \tfrac{1}{2} = 0 \quad \text{at} \quad z = \tfrac{1}{2} \pm \tfrac{1}{2}. \tag{2.3b}$$

Taking the curl of (2.1*b*) we obtain

$$\mathrm{D}^4 \frac{\psi}{r} + R\frac{\partial \theta}{\partial r} = 0 \quad \text{with} \quad \mathrm{D}^2 = \frac{\partial}{\partial r}\frac{1}{r}\frac{\partial}{\partial r} r + \frac{\partial^2}{\partial z^2}. \tag{2.4}$$

The steady solution in the asymptotic limit of large R of (2.1) is characterized by a rising (or descending) plume at $r = 0$ and a descending (or rising) cylindrical sheet at $r = \lambda$. In addition there are thermal boundary layers at $z = 0, 1$. The ring-like core enclosed by these structures is isothermal and obeys (2.4) with vanishing $\partial\theta/\partial r$. We thus obtain as a solution

$$\psi = \sum_{n=1}^{\infty} \sin(n\pi z)[A_n F_n(r, \lambda) + B_n G_n(r, \lambda)], \tag{2.5}$$

where the functions

$$F_n(r,\lambda) = r^2 K_0(n\pi r) - \lambda r \frac{K_0(n\pi\lambda)}{I_1(n\pi\lambda)} I_1(n\pi r), \tag{2.6a}$$

$$G_n(r,\lambda) = r^2 \frac{I_0(n\pi r)}{I_0(n\pi\lambda)} - \lambda r \frac{I_1(n\pi r)}{I_1(n\pi\lambda)} \tag{2.6b}$$

have been introduced which satisfy the conditions $\psi = 0$ at $r = 0, \lambda$. I_n, K_n are modified Bessel functions. The z-dependence of ψ has been chosen such that the boundary conditions for the velocity field at $z = 0, 1$ are satisfied. The coefficients A_n, B_n must be determined in such a way that the viscous stresses exerted by the interior flow at the boundaries $r \to 0$ and $r \to \lambda$ are balanced by the buoyancy forces of rising hot or the falling cold fluid at those places. For mathematical convenience we shall adopt the case of a rising plume at $r = 0$. Because of the symmetry of the problem, the solution can easily be transformed to the case of a descending plume.

Similar arguments as used in the two-dimensional problem are available for estimating the orders of magnitude of characteristic quantities. Since the aspect ratio λ is assumed to take a value of $O(1)$, the longitudinal velocities in the horizontal boundary layers and the perimeter plume have the same order of magnitude as the core flow velocity, f say, and the thicknesses of these layers assume the same order of magnitude, δ. The balance between heat conduction and convection there yields the relation $f \sim \delta^{-2}$. In addition we have the relation $f \sim R\delta$, which shows that the buoyancy force acting in the perimeter plume balances with the shearing force from the core flow. From these two relations we find that $f \sim R^{\frac{2}{3}}$ and $\delta \sim R^{-\frac{1}{3}}$, the same dependences on R as in two-dimensional convection, as previously pointed out by Jones, Moore & Weiss (1976). Nothing more definitive, however, can be said *a priori* about the orders of magnitude of the central plume velocity, $\overline{W}$, and its radius, ϵ, except for the relationship

$$\overline{W} \sim R^{\frac{1}{3}} \epsilon^{-2} \tag{2.7}$$

which follows from the fact that the mass flux passing any cross-section of the central plume, $\pi\epsilon^2\overline{W}$, is of the same order of magnitude as the corresponding quantity of the perimeter plume, $2\pi\lambda\delta f$. We note that the order of magnitude of the isothermal core flow stream function (2.5), and thereby the coefficients A_n and B_n, are at most of $O(R^{\frac{2}{3}})$.

The effectiveness of convection is measured by the Nusselt number

$$Nu = -\frac{2}{\lambda^2}\int_0^\lambda \frac{\partial\theta}{\partial z}(r,1)\, r\,\mathrm{d}r = -\frac{2}{\lambda^2}\int_0^\lambda \frac{\partial\theta}{\partial z}(r,0)\, r\,\mathrm{d}r, \tag{2.8}$$

which has a one-third power dependence on R as is easily proven from the above arguments.

The following analysis proceeds by focusing attention first on the vertical thermal layers. The solutions for the two-dimensional case (Roberts 1979; Olson & Corcos 1980) can be used as a guide, but the plume at $r = 0$ requires special consideration. As a consequence of the loss of symmetry between rising and descending motion the interior temprature differs from zero and enters the analysis as an additional parameter. Similarly, the heat transport carried by the rising plume differs significantly from that of the descending sheet. Both effects depend on the aspect ratio λ of the convection cell.

The horizontal boundary layers are more closely related to those of the two-dimensional problem and the main difference arises from the divergence of the

horizontal component of the velocity and from the different matching considerations with the centre plume.

3. Analysis of the central plume

The asymptotic solution in the neighbourhood of $r = 0$ is characterized by strong variations in the r-direction except near the boundaries $z = 0, 1$. This can be seen easily if we introduce the stretched variables $r_* = r/\epsilon$ and $u_* = u/\epsilon$ and rewrite (2.1) in terms of them. In particular, the z-component of (2.1b) reduces to

$$\frac{1}{r_*}\frac{\partial}{\partial r_*} r_* \frac{\partial w}{\partial r_*} + \epsilon^2 R(\theta - \theta_c) = 0 \tag{3.1}$$

at the lowest order of ϵ, where θ_c denotes the temperature in the isothermal core region. By integrating once we find

$$r\frac{\partial w}{\partial r} = -\epsilon^2 R \int_0^{r_*} (\theta - \theta_c)\, r'_*\, \mathrm{d}r'_* \tag{3.2a}$$

and by integrating twice we obtain

$$w = W(z) - \epsilon^2 R\left[\int_0^{r_*} (\theta - \theta_c)\, r'_*\, \mathrm{d}r'_* \ln r_* - \int_0^{r_*} (\theta - \theta_c)\, r'_* \ln r'_*\, \mathrm{d}r'_*\right] \tag{3.2b}$$

where $W(z)$ denotes the vertical velocity along the axis $r = 0$.

Solution (3.2) must be matched with the interior solution (2.5) in the overlapping region between the central plume and the isothermal core as ϵ tends to zero. From (2.5) expressed in terms of the stretched coordinate r_* we obtain, at the lowest order of ϵ,

$$r\frac{\partial w}{\partial r} = r\frac{\partial}{\partial r}\frac{1}{r}\frac{\partial \psi}{\partial r} = -2\sum_{n=1}^{\infty} A_n \sin(n\pi z), \tag{3.3a}$$

$$w = \frac{1}{r}\frac{\partial \psi}{\partial r} = 2\sum_{n=1}^{\infty} A_n(-\ln\epsilon)\sin(n\pi z). \tag{3.3b}$$

The matching between (3.2a) and (3.3a) requires that the coefficient A_n is a quantity of $O(\epsilon^2 R)$. Since the second term on the right-hand side of (3.2b) is of $O(\epsilon^2 R)$, (3.3b) should be matched with the first term on the right-hand side of (3.2b). That is, w in (3.2b) is approximated by $W(z)$ across the plume. Therefore, we find from the continuity of the heat flux

$$W 2\pi\epsilon \int_0^{\infty} (\theta - \theta_c)\, r_*\, \mathrm{d}r_* = \gamma\pi\lambda^2 Nu = \frac{1}{R} 2\pi W\left(-r\frac{\partial w}{\partial r}\right)_{r\to 0}, \tag{3.4}$$

where γ is the fraction of the heat flux which passes through the central plume. Substitution of (3.3) into (3.4) leads to

$$\frac{2\pi}{R}(-\ln\epsilon)\left[2\sum_{n=1}^{\infty} A_n \sin(n\pi z)\right]^2 = \gamma\pi\lambda^2 Nu, \tag{3.5}$$

which determines A_n as

$$A_n = \left(\frac{\gamma\lambda^2 RNu}{2(-\ln\epsilon)}\right)^{\frac{1}{2}} \frac{1-(-1)^n}{\pi n}, \tag{3.6}$$

that is, the velocity is uniform throughout the plume and given by

$$W = (\tfrac{1}{2}\gamma\lambda^2(-\ln\epsilon)\,RNu)^{\frac{1}{2}}. \tag{3.7}$$

Combining (3.7) with (2.7) we obtain an estimate for the order of magnitude of the plume radius, ϵ:

$$\epsilon(-\ln\epsilon)^{\frac{1}{4}} \sim R^{-\frac{1}{6}} \tag{3.8}$$

which shows that the radius of the central plume is much greater than the thermal boundary-layer thickness. As a result, conduction of heat in the radial direction is small in comparison with the advection of heat in the vertical direction. The plume is thus purely convective and the temperature profile at the beginning of the central plume is advected to its end invariantly. Besides the peculiar flow property embodied in (3.7) this is another distinctive property of the central plume.

The above state is valid over almost the entire length of the plume, but the situation will be different at both ends. In the remainder of this section we shall analyse the corner flow realized at both ends of the central plume and then examine the connection between the central plume and the horizontal thermal boundary layers.

Substituting (3.6) into (2.5) we consider the asymptotic form of the first term on the right-hand side as z tends to zero (or unity). The infinite sum can be transformed into an integral form and we obtain the expression

$$\begin{aligned}\psi &= \left(\frac{\gamma\lambda^2 RNu}{2(-\ln\epsilon)}\right)^{\frac{1}{2}}\frac{1}{\pi}\rho^2\sin^2\phi\int_0^\infty \frac{\sin(s\cos\phi)\,K_0(s\sin\phi)}{s}\,\mathrm{d}s \\ &= -\frac{1}{2}\left(\frac{\gamma\lambda^2 RNu}{2(-\ln\epsilon)}\right)^{\frac{1}{2}}\rho^2\sin^2\phi\ln(\tan\tfrac{1}{2}\phi),\end{aligned} \tag{3.9}$$

where ρ denotes the radial distance from the origin and ϕ the angle measured from the z-axis. In terms of the cylindrical coordinates, (3.9) is rewritten as

$$z = r\sinh\left[-2\left(\frac{2(-\ln\epsilon)}{\gamma\lambda^2 RNu}\right)^{\frac{1}{2}}\frac{\psi}{r^2}\right]. \tag{3.10}$$

Streamlines calculated from the above equation are depicted in figure 2. The vertical velocity diverges logarithmically around the centre axis, so that it can match the central plume flow. The range in which the vertical velocity takes values greater than $O(R^{\frac{2}{3}}(-\ln\epsilon)^{\frac{1}{2}})$ is restricted within a conical region with an angle of $O(\epsilon)$. Outside, the vertical velocity decreases to zero to satisfy the boundary condition at the bottom (top) surface. Near $r = 0$ the horizontal surface velocity takes a value of $O(R^{\frac{2}{3}}/(-\ln\epsilon)^{\frac{1}{2}})$. Although (3.9) provides a monotonically decreasing surface velocity distribution in r, the actual surface velocity increases with r gradually from the above limiting value since the flow component with B_n neglected in the derivation of (3.9) becomes significant as r increases.

Equation (3.9) with ψ of $O(R^{\frac{1}{3}})$ can be used to determine the size of the corner region. Assuming a pill-box-shaped region, we estimate its height and radius to be of $O(-\epsilon\ln\epsilon)$ and $O(\epsilon)$, respectively. With such scales we may evaluate the orders of magnitude of both sides in (2.1*b*, *c*) to show that the buoyancy force is of the same order as the viscous force but that the convection term is greater than the conduction term by a factor of $O(R^{\frac{1}{3}})$. Therefore, in most of the corner region the flow turns around the corner without variations of the temperature along each streamline.

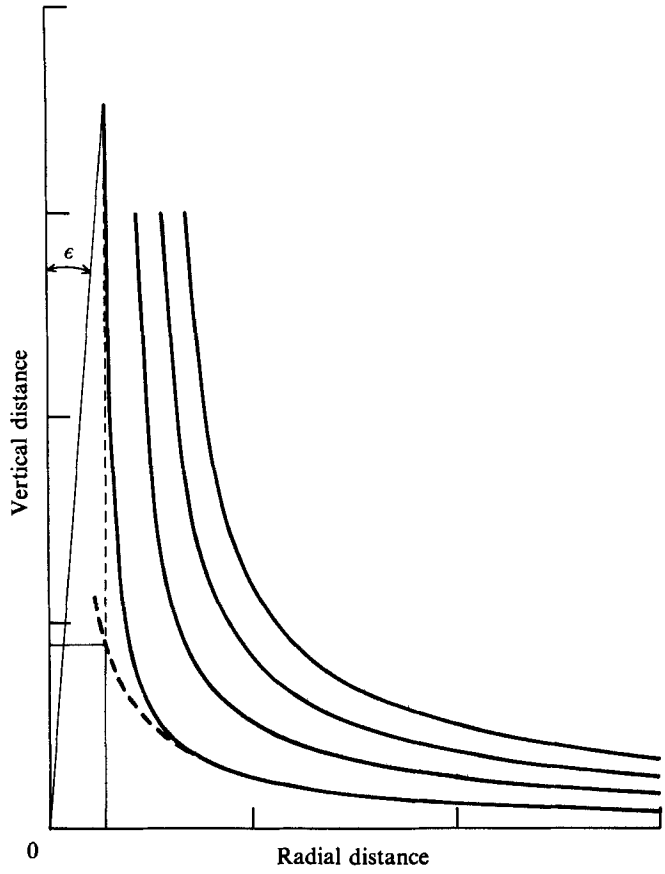

FIGURE 2. Corner flow at both ends of central plume.

There is, of course, a sublayer at the surface where heat conduction becomes significant.

At the corner A′ of figure 1 where fluid having travelled along the bottom surface approaches and changes its flow direction, the fluid near the surface has the same temperature as the bottom surface with vanishingly small temperature gradient. On the other hand, at the corner A″, where hot fluid impinges on the cold surface, a stagnation-point thermal boundary layer is formed on the top surface. Remembering that the surface velocity is of $O(R^{\frac{2}{3}}/(-\ln\epsilon)^{\frac{1}{2}})$, the thickness of this thermal boundary layer is estimated to be of $O(R^{-\frac{5}{12}}(-\ln\epsilon)^{\frac{1}{6}})$, which is smaller than the asymptotic horizontal thermal boundary-layer thickness by a factor of $O(R^{-\frac{1}{12}}(-\ln\epsilon)^{\frac{1}{6}})$. Putting $z' = 1-z$, the temperature within the stagnation-point thermal boundary layer, which is governed by the equation

$$\left(\frac{\gamma\lambda^2 RNu}{2(-\ln\epsilon)}\right)^{\frac{1}{2}}\left[\frac{\partial\theta}{\partial r}-\frac{z'}{r}\frac{\partial\theta}{\partial z}\right]=\frac{\partial^2\theta}{\partial z'^2}, \tag{3.11}$$

is given by

$$\theta=-\tfrac{1}{2}+\left(\frac{2}{\pi}\right)^{\frac{1}{2}}\int_0^{\eta}\mathrm{e}^{-\frac{1}{2}\eta^2}\,\mathrm{d}\eta,\ \eta=\left[\frac{3}{2}\left(\frac{\gamma\lambda^2 RNu}{2(-\ln\epsilon)}\right)^{\frac{1}{2}}\right]^{\frac{1}{2}}\frac{z'}{r^{\frac{1}{2}}}. \tag{3.12}$$

Around the corner A′ the flow near the bottom surface is described by the following approximate form of the stream function (2.5):

$$\psi = \left(\frac{\gamma\lambda^2 RNu}{2(-\ln\epsilon)}\right)^{\frac{1}{2}} rz + \left[\left(\frac{\gamma\lambda^2 RNu}{2(-\ln\epsilon)}\right)^{\frac{1}{2}} f_2(\lambda) + (\tfrac{1}{2}(1-\gamma)\,\lambda RNu)^{\frac{1}{2}} g_1(\lambda)\right] r^2 z, \tag{3.13}$$

where

$$f_2(\lambda) = \sum_{n\,\mathrm{odd}} n\pi\lambda \frac{K_0(n\pi\lambda)}{I_1(n\pi\lambda)}, \tag{3.14a}$$

$$g_2(\lambda) = \sum_{n=1}^{\infty} n\pi B_n \left[\frac{n\pi\lambda}{2I_1(n\pi\lambda)} - \frac{1}{I_0(n\pi\lambda)}\right]. \tag{3.14b}$$

With $\psi \sim O(R^{\frac{1}{3}})$ we identify this with part of a closed streamline which surrounds the isothermal core region. Equation (3.13) suggests that the boundary streamline is switched from the first term on the right-hand side to the second term at a distance $r = r_c$ which is given by

$$r_c \sim \frac{\left(\frac{\gamma}{1-\gamma}\frac{\lambda}{(-\ln\epsilon)}\right)^{\frac{1}{2}} \frac{1}{g_1}}{1+\left(\frac{\gamma}{1-\gamma}\frac{\lambda}{(-\ln\epsilon)}\right)^{\frac{1}{2}} \frac{f_2}{g_1}}. \tag{3.15}$$

For λ of $O(1)$ this leads to

$$r_c \sim O\left(\frac{1}{(-\ln\epsilon)^{\frac{1}{2}}}\right). \tag{3.16}$$

The same relationship holds for the top surface. Hence, using (3.12) the heat flux across the surface $r \leqslant r_c$ is evaluated as follows:

$$2\pi \int_0^{r_c} \left.\frac{\partial\theta}{\partial z}\right|_{z=0} r\,\mathrm{d}r = -\frac{4(2\pi)^{\frac{1}{2}}}{3}\left[\frac{3}{2}\left(\frac{\gamma\lambda^2 RNu}{2(-\ln\epsilon)}\right)^{\frac{1}{2}}\right]^{\frac{1}{2}} r_c^{\frac{3}{2}} = O\left(\frac{R^{\frac{1}{3}}}{-\ln\epsilon}\right). \tag{3.17}$$

For large R this flux is asymptotically negligible in comparison with the net heat flux across the top surface. Furthermore, it is found from (3.13) that the thickness of the horizontal thermal boundary layer which emerges from the stagnation-point thermal boundary layer grows to a thickness comparable with the average thickness of $O(R^{-\frac{1}{3}})$ at the distance $r \sim r_c$.

4. The perimeter plume

The basic balances describing the perimeter plume are given by the stress exerted by the descending plume,

$$\frac{\partial w}{\partial r}(\lambda, z) = R\delta \int_0^{\infty} (\theta - \theta_c)\,\mathrm{d}x_*, \tag{4.1}$$

and by the continuity of the heat flux

$$W(\lambda, z)\, 2\pi\lambda\delta \int_0^{\infty} (\theta - \theta_c)\,\mathrm{d}x_* = (1-\gamma)\,\pi\lambda^2 Nu, \tag{4.2}$$

where $x_* = (\lambda - r)/\delta$, and $\delta = R^{-\frac{1}{3}}$ denotes the thickness of the plume. By combining (4.1) and (4.2) we obtain as a boundary condition for w at $r = \lambda$:

$$w(\lambda, z)\frac{\partial w}{\partial r}(\lambda, z) = \tfrac{1}{2}(1-\gamma)\,\lambda RNu. \tag{4.3}$$

Since the coefficients A_n are smaller by the factor $(-\ln\epsilon)^{\frac{1}{2}}$ than the coefficients B_n according to (3.6) and (4.3), we can neglect the coefficients A_n at $r = \lambda$ and rewrite (4.3) in the form

$$\left[\sum_{n=1}^{\infty} \hat{B}_n G_n'(\lambda) \sin(n\pi z)\right]\left[\sum_{n=1}^{\infty} \hat{B}_n G_n''(\lambda) \sin(n\pi z)\right] = 1, \tag{4.4}$$

where we have defined

$$\hat{B}_n := -B_n \left(\frac{2}{(1-\gamma)\lambda RNu}\right)^{\frac{1}{2}} \tag{4.5}$$

and

$$G_n'(\lambda) := 2 + n\pi\lambda\left[\frac{I_1(n\pi\lambda)}{I_0(n\pi\lambda)} - \frac{I_0(n\pi\lambda)}{I_1(n\pi\lambda)}\right], \tag{4.6a}$$

$$G_n''(\lambda) := 2n\pi \frac{I_1(n\pi\lambda)}{I_0(n\pi\lambda)}. \tag{4.6b}$$

Equation (4.4) provides the determining equation for the coefficients $\hat{B}_n$, which is solved numerically. Nevertheless, we can solve it analytically for special cases. Since the results are useful for later discussion we mention them here briefly.

In the limiting cases of $\lambda \to \infty, 0$ the quantities G_n' and G_n'' in (4.6) assume the form

$$G_n' \to 1, \quad G_n'' \to 2n\pi \quad \text{as} \quad \lambda \to \infty, \tag{4.7a}$$

$$G_n' \to \tfrac{1}{4}(n\pi\lambda)^2, \quad G_n'' \to (n\pi)^2\lambda \quad \text{as} \quad \lambda \to 0. \tag{4.7b}$$

From (4.4) and (4.7*a*), $\hat{B}_n$ approaches a value independent of λ as λ tends to infinity. This property will be utilized to examine the asymptotic behaviour of Nu for large aspect ratios. On the other hand, for small λ we obtain the expression

$$\hat{B}_n = \frac{4}{\lambda^{\frac{3}{2}}} \frac{1-(-1)^n}{(n\pi)^3} \tag{4.8}$$

which leads to a parabolic form of plume velocity, $W(z)$, and a uniform shearing rate, $\partial W/\partial x_*$. Furthermore, the validity of (4.4) near $z = 0, 1$ requires n to be odd in general.

As the perimeter plume approaches the bottom surface it widens. The width of the plume at the point where u and w are of the same magnitude is of $O(R^{-\frac{2}{5}})$. This estimate is obtained from the property that, according to the solution of (4.4), $W(\lambda, z)$ varies like $z^{\frac{1}{2}}$ as the boundary $z = 0$ is approached (see also Roberts 1979). Hence the scale δ_c of the corner region is governed by the relationship $R^{-\frac{1}{3}}R^{\frac{2}{3}} = \delta_c \delta_c^{\frac{1}{2}} R^{\frac{2}{3}}$, which expresses the approximate equality of fluid fluxes inside the plume above the corner and in the corner itself. The order of magnitude $R^{-\frac{2}{5}}$ of δ_c indicates that heat conduction is not important in the corner and that the temperature distribution is changed only through advection inside the region.

Conduction becomes dominant, of course, right at the boundary $z = 0$. A thin layer of thickness δ_1 must be considered separately. Using the balance between vertical advection and conduction in this layer we estimate from the balance

$$-\delta_1^{\frac{1}{2}} R^{\frac{2}{3}} \frac{z}{\delta_1} \frac{\partial\theta}{\partial z} \approx \frac{\partial^2\theta}{\partial z^2} \tag{4.9}$$

that δ_1 must be of $O(R^{-\frac{4}{5}})$. This estimate is likely to be a lower bound since the square-root dependence of $w(\lambda, z)$ may not be valid down to the distance δ_1 from the bottom surface. However, the exact order of magnitude is not important for the following as long as δ_1 is small compared to $R^{-\frac{1}{3}}$. Even if a linear dependence on z up to $z = \delta_c$ is

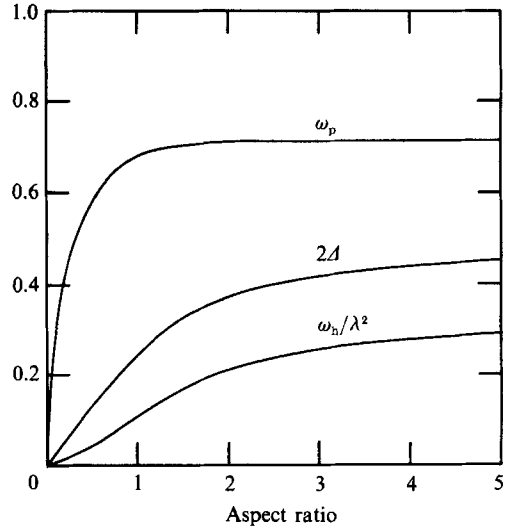

FIGURE 3. Surface velocity integrals as functions of the aspect ratio.

assumed the estimate for δ_1 is changed only to $R^{-\frac{7}{18}}$, and in either case the heat flux across the surface in the corner is found to be negligible.

5. Thermal structure in the boundary layers

Each boundary layer is so thin that flow is unidirectional within it, that is, the longitudinal velocity at any cross-section is uniform and given by the boundary value of the core flow. Because of this flow property the analysis of thermal structure in the boundary layers can be reduced to the so-called second kind of Stokes problem by use of the von Mises transformation, as described below.

Using the stream function ψ as the transverse coordinate, we can transform the boundary-layer type of heat equation (2.1c) into

$$\frac{\partial \Theta}{\partial t} = \frac{\partial^2 \Theta}{\partial x^2} \tag{5.1}$$

where for mathematical convenience the temperature θ has been replaced by $\Theta = \theta - \theta_c$ and the coordinate

$$x = (2\Omega_h + \lambda^2 \Omega_p)^{-\frac{1}{2}} \psi \tag{5.2}$$

has been introduced. The downstream coordinate along the cell edge, t, is defined in the respective layers as follows.

$$(2\Omega_h + \lambda^2 \Omega_p)\, t = \begin{cases} \displaystyle\int_0^r r^2 u(r, 1)\, \mathrm{d}r & \text{in the top layer,} \\ \Omega_h + \lambda^2 \displaystyle\int_1^z w(\lambda, z)\, \mathrm{d}z & \text{in the perimeter plume,} \\ \Omega_h + \lambda^2 \Omega_p + \displaystyle\int_\lambda^r r^2 u(r, 0)\, \mathrm{d}r & \text{in the bottom layer.} \end{cases} \tag{5.3}$$

The quantities Ω_h and Ω_p appearing in (5.2) and (5.3) denote the surface velocity

integrals defined in (5.4) and (5.5) below, and shown in figure 3. In those integrals the contributions from the flow component with the coefficients A_n may be neglected. The limiting forms in (5.4*b*) and (5.5*b*) are due to (4.7*b*) and (4.8).

$$\Omega_{\rm h} = \int_0^{\lambda} r^2 u(r,1)\,{\rm d}r = \int_{\lambda}^{0} r^2 u(r,0)\,{\rm d}r$$
$$\equiv (\tfrac{1}{2}(1-\gamma)\,\lambda RNu)^{\frac{1}{3}}\omega_{\rm h}(\lambda), \tag{5.4a}$$

with

$$\omega_{\rm h}(\lambda) = 2\lambda^3 \sum_{n\,\text{odd}} \left[\frac{I_1(n\pi\lambda)}{I_0(n\pi\lambda)} - \frac{2I_2(n\pi\lambda)}{n\pi\lambda I_0(n\pi\lambda)} - \frac{I_2(n\pi\lambda)}{I_1(n\pi\lambda)}\right]\hat{B}_n$$
$$\to \begin{cases} +\dfrac{2\lambda^2}{\pi} \displaystyle\sum_{n\,\text{odd}} \dfrac{\hat{B}_n}{n} & \text{as} \quad \lambda \to \infty, \\ \dfrac{16\lambda^{\frac{7}{2}}}{\pi} \displaystyle\int_0^{\infty} \dfrac{1}{s^3}\left[\dfrac{I_1(s)}{I_0(s)} - \dfrac{2I_2(s)}{sI_0(s)} - \dfrac{I_2(s)}{I_1(s)}\right]{\rm d}s & \text{as} \quad \lambda \to 0, \end{cases} \tag{5.4b}$$

and

$$\Omega_{\rm p} = \int_1^{0} w(\lambda, z)\,{\rm d}z \equiv (\tfrac{1}{2}(1-\gamma)\,\lambda RNu)^{\frac{1}{3}}\omega_{\rm p}(\lambda), \tag{5.5a}$$

with

$$\omega_{\rm p}(\lambda) = 4 \sum_{n\,\text{odd}} \frac{1}{n\pi}\left[2 + n\pi\lambda\left\{\frac{I_1(n\pi\lambda)}{I_0(n\pi\lambda)} - \frac{I_0(n\pi\lambda)}{I_1(n\pi\lambda)}\right\}\right]\hat{B}_n$$
$$\to \begin{cases} \dfrac{4}{\pi} \displaystyle\sum_{n\,\text{odd}} \dfrac{\hat{B}_n}{n} & \text{as} \quad \lambda \to \infty, \\ \lambda^{\frac{1}{2}} & \text{as} \quad \lambda \to 0. \end{cases} \tag{5.5b}$$

The boundary conditions for (5.1) are

$$\Theta(0 < t < \Delta, x = 0) = -\tfrac{1}{2} - \theta_{\rm c}, \tag{5.6a}$$

$$\frac{\partial \Theta}{\partial x}(\Delta < t < 1-\Delta, x = 0) = 0, \tag{5.6b}$$

$$\Theta(1-\Delta < t < 1, x = 0) = \tfrac{1}{2} - \theta_{\rm c}, \tag{5.6c}$$

$$\Theta(t = 0, x) = \Theta(t = 1, x), \tag{5.6d}$$

$$\Theta(t, x \to \infty) \to 0, \tag{5.6e}$$

where

$$\Delta(\lambda) = \frac{\omega_{\rm h}}{2\omega_{\rm h} + \lambda^2 \omega_{\rm p}}. \tag{5.7}$$

Since the temperature profiles at both ends of the central plume are identical, the solution is periodic in t with unit period. From the assumption of steadiness we obtain the condition

$$q \equiv \int_0^{\Delta} \frac{\partial \Theta}{\partial x}(t, x = 0)\,{\rm d}t = -\int_{1-\Delta}^{1} \frac{\partial \Theta}{\partial x}(t, x = 0)\,{\rm d}t, \tag{5.8}$$

which determines the unknown core temperature $\theta_{\rm c}$ as a function of Δ. The central plume heat flux fraction γ is calculated from

$$\gamma q = \int_0^{\infty} \Theta(t = 0, x)\,{\rm d}x. \tag{5.9}$$

The Nusselt number Nu is derived from

$$R^{-\frac{1}{3}}Nu = 2q^{\frac{4}{3}}(1-\gamma)^{\frac{1}{3}}\left(2\frac{\omega_h}{\lambda^2}+\omega_p\right)^{\frac{2}{3}}\lambda^{-1}. \tag{5.10}$$

From (5.8), (5.9) and (5.10) the quantities θ_c, γ and $R^{-\frac{1}{3}}Nu$ are determined as functions of Δ. To obtain their dependences on λ, (5.7) with (5.4b) and (5.5b) must be invoked, which yields Δ as a monotonically increasing function of λ. According to the limiting value in (5.4b) and (5.5b), $\lambda^2\omega_p = 2\omega_h$ holds in the limit $\lambda\to\infty$. Therefore, Δ lies in the range between 0 and $\frac{1}{4}$.

For prescribed values of θ_c and Δ, (5.1) can be solved numerically by starting with an arbitrary temperature profile at $t = 0$ and marching forward in t and applying the boundary conditions (5.6) in cyclic order. The determination of θ_c by (5.8), however, may contain significant errors because convergence of the far field is inevitably slow even if the near field appears to converge fast. In fact, since for any value θ_c that does not satisfy (5.8), there will be a net heat flux towards infinity, slow convergence of the far field makes it difficult to determine an accurate value of θ_c. To eliminate this difficulty we next consider the general property which the exact solution should satisfy. This will lead to an alternative formula which is also suitable for the calculation of the fraction of the heat flux carried by the central plume.

As shown in Appendix B, the solution must satisfy the following relations:

$$\int_0^1 \frac{\partial\Theta}{\partial x}(t, x=0)\,\mathrm{d}t = 0, \tag{5.11a}$$

$$\int_0^1 \Theta(t, x=0)\,\mathrm{d}t = 0, \tag{5.11b}$$

$$\gamma q = -\int_0^1 \frac{\partial\Theta}{\partial x}(t, x=0)\,t\,\mathrm{d}t. \tag{5.11c}$$

The first equation (5.11a) is nothing other than the steadiness condition (5.8). The second equation is expressed in terms of the original variables as follows:

$$\oint \theta \boldsymbol{V}\cdot\mathrm{d}\boldsymbol{l} = \theta_c \oint \boldsymbol{V}\cdot\mathrm{d}\boldsymbol{l}, \tag{5.12}$$

indicating that the core temperature coincides with the average value of the surface temperature weighted by the surface velocity. This equation is of the same form as that which Batchelor (1956) derived for determining the value of core vorticity in high-Reynolds-number flow with closed streamlines. The third equation is more convenient than (5.9) in that the integration is changed to that over the boundary. Actual numerical calculations show that for a given Δ the variation of the residual of (5.8) with θ_c is small after several iterations while the left-hand side of (5.11b) still varies strongly. Thus, (5.11b) can be used as a criterion to find the accurate θ_c-value.

Although Δ does not exceed $\frac{1}{4}$ in the present analysis, (5.1) together with (5.6) has a continuous solution in the range $0 \leqslant \Delta \leqslant \frac{1}{2}$. For the extreme cases of $\Delta = 0, \frac{1}{2}$ it is not difficult to solve the equation analytically. The calculated numerical solution provides good agreement with the thus-obtained approximate analytical solution for the characteristic quantities q, θ_c, γ and θ_1 as functions of Δ, where $\theta_1 = \theta(t\to\Delta, x = 0)$ denotes the surface temperature at the end of the perimeter plume and the difference $\theta_1 + \frac{1}{2}$ characterizes the effect of heat conduction within the perimeter plume.

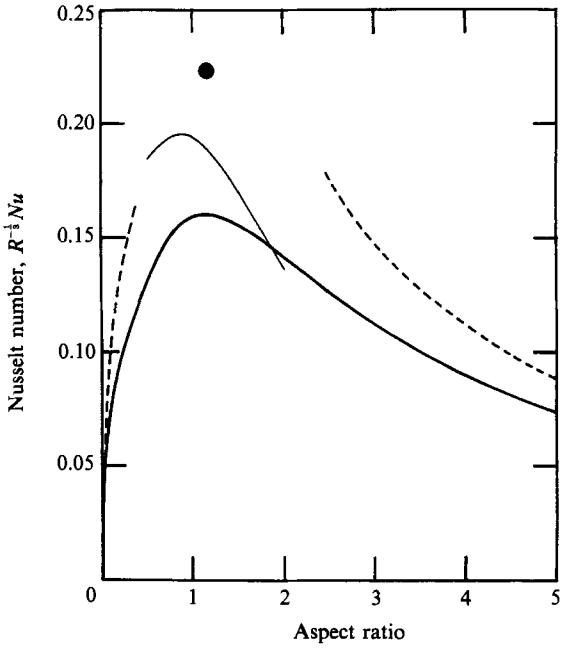

FIGURE 4. Nusselt number dependence on the aspect ratio. The two broken lines indicate the asymptotes $0.448/\lambda$ at large aspect ratio and $0.229\lambda^{\frac{1}{3}}$ at small aspect ratio. The thin line denotes the result by Olson (1987) for two-dimensional convection. The maximum point in Jones *et al.*'s (1976) numerical calculation is shown by the solid circle.

6. Results and discussion

Figure 4 shows the variation of $R^{-\frac{1}{3}}Nu$ with λ. The corresponding curve for the two-dimensional case has also been drawn for comparison. Although both curves are of similar form, there are some significant differences between them. In contrast to a finite value of $R^{-\frac{1}{3}}Nu$ at $\lambda = 0$ in the two-dimensional case, $R^{-\frac{1}{3}}Nu$ decreases to zero like $\lambda^{\frac{1}{3}}$ in the three-dimensional case. As we shall see later, this property is caused by the fact that the central-plume heat flux fraction γ tends to unity as $\lambda \to 0$. Another notable difference is observed in the behaviour at large aspect ratio. In the two-dimensional case the curve approaches a decay proportional to λ^{-1} for λ greater than 2. In the three-dimensional case a similar property holds for the limit $\lambda \to \infty$, but the approach to the asymptote is much slower. This difference comes from the difference in the asymptotic form of the surface velocity integrals for the two cases. In the two-dimensional case they approach constant values exponentially with increasing λ, whereas in the three-dimensional case deviations from their limiting values are inversely proportional to λ. Such a slow decay of $R^{-\frac{1}{3}}Nu$ for large aspect ratios implies that even though the two-dimensional value of $R^{-\frac{1}{3}}Nu$ is greater than the three-dimensional value of $R^{-\frac{1}{3}}Nu$ around $\lambda = 1$ the latter may exceed the former at large aspect ratios. In view of the upper limit for λ given in Appendix A this possibility, however, does not seem to occur in reality. The solid circle in figure 4 indicates the maximum point of the numerical calculation by Jones *et al.* (1976) for $R = 65600$. This value is about 1.4 times greater than the present result, although their positions as a function of λ agree. Further, according to Jones *et al.* the maximum value of Nu for the three-dimensional case was a little smaller than that of the two-dimensional case. This tendency is the same although the difference is larger.

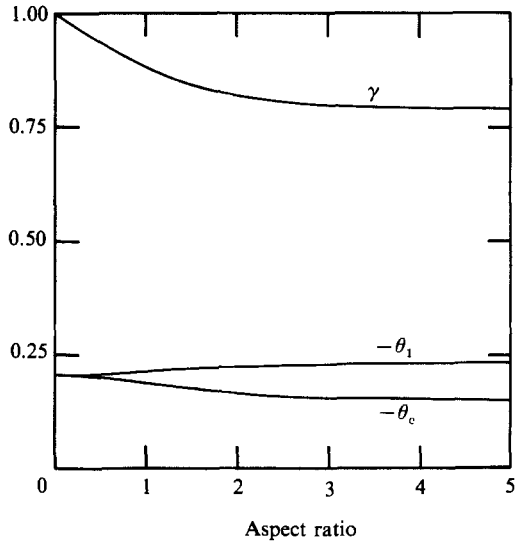

FIGURE 5. Several properties as functions of the aspect ratio: plume heat flux fraction γ; stagnation temperature at perimeter plume end θ_1; and core temperature θ_c. In the rising-central-plume case the two temperatures take negative values. They approach the limiting value $1/\sqrt{2}-\frac{1}{2}$ at vanishing aspect ratio and the asymptotes -0.14 and -0.27 at large aspect ratio. The central heat flux fraction becomes unity at vanishing aspect ratio and decreases to 0.76 with increasing aspect ratio.

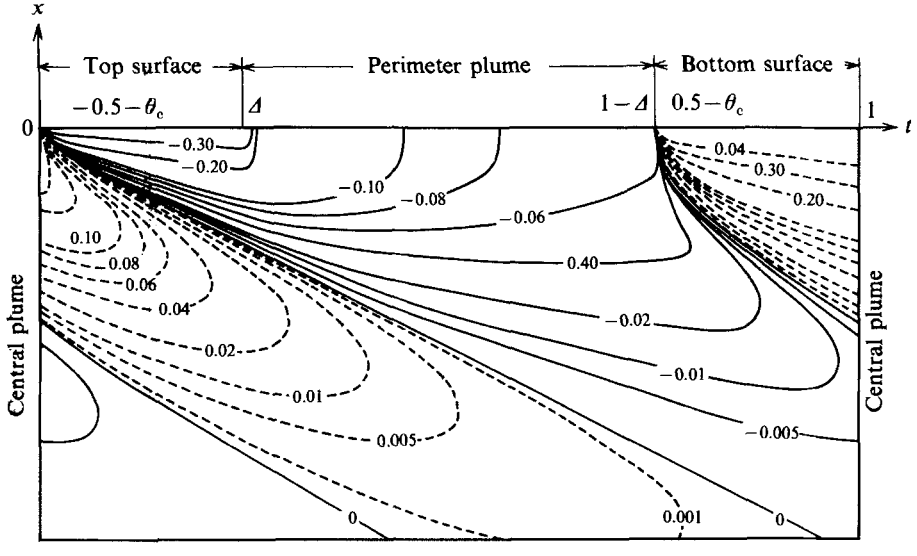

FIGURE 6. Isotherms in thermal boundary layers. An example of the solution to the equation system (5.1), (5.6) and (5.8). Since the central plume is convection-dominant, the temperature profile at the end of the bottom layer is the same as that at the start of the top layer.

Consistent with Jones *et al.*'s result the core temperature, θ_c, for the case of an ascending central plume becomes negative as shown in figure 5. It increases from the limiting value $\frac{1}{2}-1/\sqrt{2}$ at $\lambda = 0$ to a constant value as λ tends to infinity. The reason why θ_c becomes negative may be understandable from figure 6, where isotherms derived from the numerical solution are depicted for the extreme case of $\Delta = \frac{1}{4}$. Since

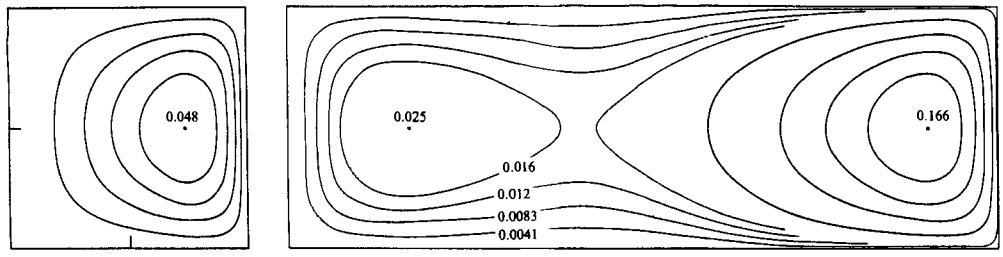

FIGURE 7. Streamlines for $\lambda = 1$ (left) and $\lambda = 3$ (right). The numbers express the values of $R^{-\frac{1}{3}}\psi$ with $R = 10^6$. The streamlines without numbers are contoured evenly between zero and the minimum stream-function value. The central and perimeter plumes are at the left and right edges, respectively.

the influence of the cell boundaries penetrates into the interior further downstream, the two θ_c-isotherms originating from the two stagnation points located at the terminal ends of both plumes continue in the form of two intertwined spirals into the core region. These curves assume the form of a vertical straight line in the region of the central plume, since the temperature profile at the beginning is invariantly advected by the vertically uniform velocity in the central plume. The asymmetry between the two plumes is also responsible for the different thicknesses of the upper and lower horizontal boundary layers which are evident in figure 6 and for the negative value of θ_c. The hot fluid tongue at the upper boundary starts with a high initial temperature but experiences a rapid decay towards the value θ_c near its end because of the small thickness of the boundary layer. The cold tongue at the lower boundary, on the other hand, starts with the moderate value θ_1 which does not change much as the cold tongue approaches the centre. In order that mean temperatures in the hot and cold horizontal tongues differ by an approximately equal absolute amount from the core temperature, the latter must assume a negative value.

Figure 7 shows streamlines of the isothermal core flow for $\lambda = 1, 3$ and $R = 10^6$. As in the two-dimensional case, two separate convection rolls driven by each plume appear when λ exceeds a critical value. The reason for this phenomenon is that the distance over which each plume can drive the flow effectively is restricted to the order of the plume height. Accordingly, at the distance where the influence of the plumes dies away the decay of the horizontal surface velocity widens the local boundary-layer thickness until a breakdown of the present analysis occurs. To see the variation with λ of the horizontal surface velocity distribution, several cases are shown in figure 8 for the same value of R as in figure 7. When λ is below a critical value, around 1.5, the distribution has a single maximum value corresponding to a single convection roll. When λ exceeds the critical value, a minimum emerges in the central part accompanied by the appearance of double rolls and the two maximum points move towards both ends. The position of the right maximum point corresponds to the location of the centre of the roll driven by the perimeter plume, which settles down at the distance $1/\pi$ away from the perimeter in the limit $\lambda \to \infty$. Since the buoyancy force acting in the perimeter plume becomes constant as λ tends to infinity, the maximum value does not change significantly with λ. The roll driven by the central plume experiences a similar fate. It can be noticed, however, that the left maximum value is an increasing function of λ while the maximum on the perimeter side is a slightly decreasing function of λ. This feature is caused by the fact that the left maximum value approaches the asymptote $(\gamma\lambda^2 RNu/2(-\ln\epsilon))^{\frac{1}{2}}$, where

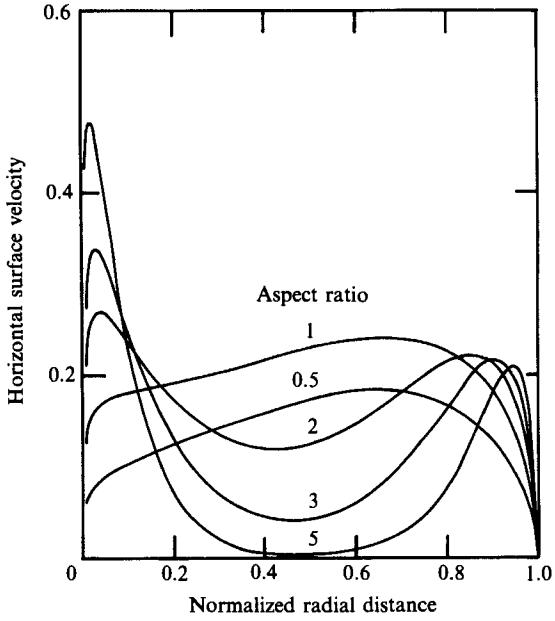

FIGURE 8. Horizontal surface velocity profiles. The development of a broad velocity minimum range, or the growth of the horizontal thermal boundary-layer thickness, is observed in the mid-region of the cell as the aspect ratio increases beyond a certain value.

Nu and γ become constant as $\lambda \to \infty$. Since λ must be much less than $O(-\ln \epsilon)$ for the validity of the present analysis (see Appendix A), this maximum value may not exceed the other one.

Figure 9 shows the distributions of vorticity at the midheight $z = \frac{1}{2}$. Characteristic of axisymmetric convection is a narrow, highly concentrated vorticity region around the central plume. This situation is easily recognized if we replace the central plume by a thin string drawn with a constant force in a viscous fluid. Since the surface area per unit length, upon which the frictional force acts, decreases with decreasing radius, the surface shearing rate increases inversely proportionally to the radius in order to provide a constant driving force. For the case of $\lambda = 1$ the vorticity is almost uniform except near the centre plume, implying that fluid rotates like a rigid body.

It is interesting to examine the variation with λ of the temperature θ_1 at the bottom of the perimeter plume. Figure 5 shows that θ_1 increases monotonically with λ. This implies that the effect of conduction becomes small as the aspect ratio increases. The behaviour of θ_1 in the extreme case $\lambda \to 0, \infty$ can be physically interpreted as follows. First we consider the reason why θ_1 coincides with θ_c in the limit $\lambda \to 0$. Since the degree of decay of the hot fluid tongue temperature depends on the distance of travel through the fluid, the horizontal temperature profile at the beginning of the perimeter plume seems to become oscillatory for small λ. In fact, the top layer has the maximum temperature $\frac{1}{2}$ at a distance of $O(\lambda^{\frac{1}{3}}R^{-\frac{1}{3}})$ from the surface, and this temperature profile is advected around the corner into the perimeter plume. Since the plume height is unity, an initial disturbance disperses over a distance of the order of the plume thickness while travelling with the plume. As a result the initial rapid temperature variation within a narrow region with a thickness of the order $\lambda^{\frac{1}{3}}R^{-\frac{1}{3}}$ is smeared out by conduction at a downstream distance of $O(\lambda^{\frac{1}{3}}R^{-\frac{1}{3}})$. At the same time this process implies that the tail of the hot fluid tongue actually decays

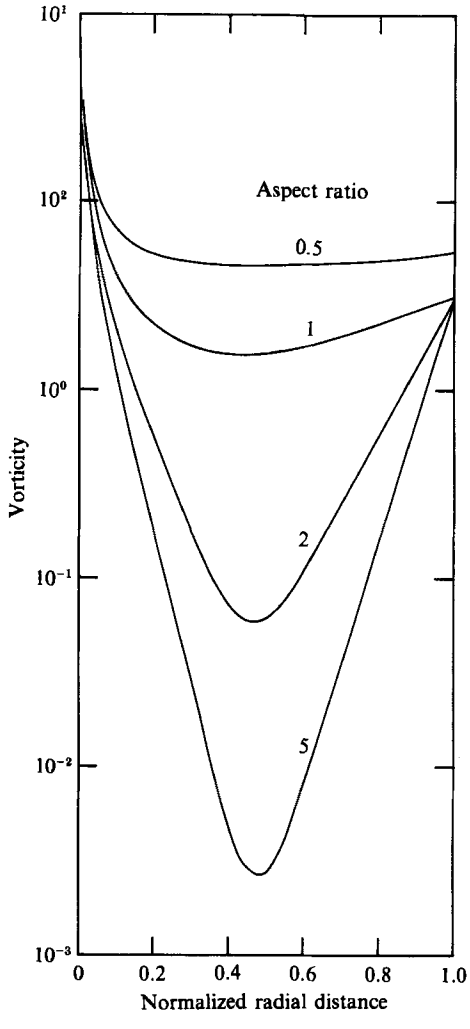

FIGURE 9. Vorticity distributions at the half-height.

rapidly to the core temperature. Thus, the temperature in the perimeter plume coincides with the core temperature except for a short initial interval and the net heat flux through the plume becomes equal to zero, i.e. $\gamma = 1$, in the limit $\lambda \to 0$. In the large-aspect-ratio limit the penetration distance of influence from the top surface increases as well as the thickness of each thermal boundary layer, while the magnitude of the surface velocity does not change significantly as we have seen before. Hence, the growth of the boundary-layer thicknesses weakens the effect of conduction and raises the value of θ_1. Both the greater deviation from θ_c and the growth of the thickness favour the increase in the net heat flux through the perimeter plume. Nevertheless, figure 5 indicates that γ is still above $\frac{3}{4}$ for the limit $\lambda \to \infty$.

That most of the heat transport occurs through the central plume even in the limit of $\lambda \to \infty$ is the most surprising aspect of the mathematical analysis. But it must be taken into account that, according to the criterion derived in Appendix A, λ may not exceed the magnitude of $\ln \ln (\epsilon^{-1})$ which imposes a very severe constraint indeed. The basic reason for the importance of the central plume is that the mass flux

participating in the perimeter plume also participates in the central plume. While the horizontal boundary-layer thickness decreases for reasons of continuity before reaching the perimeter plume, it increases rapidly for the same reason before merging with the central plume. The geometric disadvantage of the latter is thus compensated by the dynamic advantage of the rising horizontal boundary layer.

This study was carried out during the first author's visit to Germany as an Alexander von Humboldt Foundation research fellow. The authors thank the Foundation deeply.

Appendix A

Although in the present analysis the aspect ratio is assumed to be of $O(1)$, the results are valid over the range described below. The upper and lower bounds on λ are derived by examining the asymptotic behaviour of (3.15) as $\lambda \to 0$ and ∞. For the limiting case of $\lambda \to 0$, (3.14) takes the form

$$f_2 \to k_2 \frac{1}{\lambda}, \quad k_2 = \frac{1}{2\pi} \int_0^\infty \frac{sK_0(s)}{I_1(s)} \mathrm{d}s, \tag{A 1a}$$

$$g_1 \to k_1 \frac{1}{\lambda^{\frac{1}{2}}}, \quad k_1 = \frac{8}{\pi} \int_0^\infty \frac{1}{s^2} \left[\frac{s}{2I_1(s)} - \frac{1}{I_0(s)} \right] \mathrm{d}s \tag{A 1b}$$

which can be substituted into (3.15) to yield

$$r_c \sim \frac{\left(\dfrac{\gamma}{1-\gamma} \dfrac{\lambda^2}{(-\ln \epsilon)} \right)^{\frac{1}{2}} \dfrac{1}{k_1}}{1 + \left(\dfrac{\gamma}{1-\gamma} \dfrac{1}{(-\ln \epsilon)} \right)^{\frac{1}{2}} \dfrac{k_2}{k_1}} \ll \lambda. \tag{A 2}$$

Since $1-\gamma = k\lambda$ for small λ (see figure 5), the last inequality gives the lower bound on λ, i.e.

$$\lambda \gg O\left(\frac{1}{-\ln \epsilon} \right). \tag{A 3}$$

For large λ (3.14) can be approximated by

$$f_2 \approx \pi \mathrm{e}^{-2\pi\lambda} \tag{A 4a}$$

$$g_1 \approx \pi^2 B_1 (\tfrac{1}{2}\pi\lambda - 1)(2\lambda)^{\frac{1}{2}} \mathrm{e}^{-\pi\lambda}. \tag{A 4b}$$

Substituting these into (3.15) we obtain

$$r_c \sim \left(\frac{\gamma}{1-\gamma} \frac{\lambda}{(-\ln \epsilon)} \right)^{\frac{1}{2}} \frac{\sqrt{2}\, \mathrm{e}^{\pi\lambda}}{B_1 \pi^3 \lambda^{\frac{3}{2}}}. \tag{A 5}$$

This must be much smaller than unity, so that

$$\frac{1}{\lambda} \mathrm{e}^{\pi\lambda} \ll \frac{\pi^3}{\sqrt{2}} B_1 \left(\frac{1-\gamma}{\gamma} (-\ln \epsilon) \right)^{\frac{1}{2}}. \tag{A 6}$$

The results presented in §6 are all based on the assumption that the contributions of the axial flow component to the surface velocity integrals, Ω_h and Ω_p, are negligible in comparison with those of the perimeter flow component. This assumption imposes

the same upper bound as (A 3) since the vertical surface velocity integral for the axial and perimetric flow components respectively take values of $O((\gamma\lambda^2 RNu/(-\ln\epsilon))^{\frac{1}{3}})$ and $O(((1-\gamma)\lambda^2 RNu)^{\frac{1}{2}})$ as λ tends to zero. On the other hand, for large λ the contribution of the axial flow component to the horizontal surface integral becomes $O((\gamma\lambda^2 RNu/(-\ln\epsilon))^{\frac{1}{3}})$, while the contribution from the perimeter flow component is proportional to the factor $((1-\gamma)\lambda RNu)^{\frac{1}{2}}$ and must be of $O(R^{\frac{1}{3}})$. Hence, we obtain the condition $\lambda \ll -\ln\epsilon$, which is automatically satisfied when (A 6) holds.

Appendix B

Operation of the Laplace transform in x transforms (5.1) into

$$\frac{\mathrm{d}\bar{\Theta}}{\mathrm{d}t} = s^2\bar{\Theta} - \frac{\partial\Theta}{\partial x}(t, x=0) - s\Theta(t, x=0). \tag{B 1}$$

This is integrated to yield

$$\bar{\Theta} = \mathrm{e}^{s^2 t}\left[-\int_0^t \left\{\frac{\partial\Theta}{\partial x}(t', x=0) + s\Theta(t', x=0)\right\}\mathrm{e}^{-s^2 t'}\,\mathrm{d}t' + C\right]. \tag{B 2}$$

From the cyclic condition (5.6*d*) one obtains

$$\int_0^\infty \Theta(t=0, x)\,\mathrm{e}^{-sx}\,\mathrm{d}x = \bar{\Theta}(t=0) = \bar{\Theta}(t=1) = \int_0^\infty \Theta(t=1, x)\,\mathrm{e}^{-sx}\,\mathrm{d}x. \tag{B 3}$$

The constant of integration, C, is thus determined by

$$C = \frac{\int_0^1 \frac{\partial\Theta}{\partial x}(t, x=0)\,\mathrm{e}^{-s^2 t}\,\mathrm{d}t + s\int_0^1 \Theta(t, x=0)\,\mathrm{e}^{-s^2 t}\,\mathrm{d}t}{1-\mathrm{e}^{-s^2}} \tag{B 4}$$

Since the net heat flux through the central plume must be finite, the equation

$$\begin{aligned}\gamma q &= \int_0^\infty \Theta(t=0, x)\,\mathrm{d}x = \bar{\Theta}(t=0; s=0) = \lim_{s\to 0} C \\ &= \lim_{s\to 0} \frac{\int_0^1 \frac{\partial\Theta}{\partial x}(t, x=0)\,\mathrm{d}t + s\int_0^1 \Theta(t, x=0)\,\mathrm{d}t - s^2\int_0^1 \frac{\partial\Theta}{\partial x}(t, x=0)\,t\,\mathrm{d}t + O(s^4)}{s^2 + O(s^4)}\end{aligned} \tag{B 5}$$

leads to the three relations (5.11).

The validity of these relations is confirmed by the separation-of-variable form of the general solution to (5.1) subject to the conditions (5.6*d*, 3):

$$\Theta = \sum_{n=1}^{\infty} \mathrm{e}^{-(n\pi x)^{\frac{1}{2}}}[P_n \cos((n\pi x)^{\frac{1}{2}} - 2n\pi t) - Q_n \sin((n\pi x)^{\frac{1}{2}} - 2n\pi t)]. \tag{B 6}$$

REFERENCES

Batchelor, G. K. 1956 *J. Fluid Mech.* **1**, 177.

Busse, F. H. 1983 *Geophys. Res. Lett.* **10**, 285.

Jones, C. A., Moore, D. R. & Weiss, N. O. 1976 *J. Fluid Mech.* **73**, 353.

Machetel, P. & Rabinowicz, M. 1985 *Geophys. Res. Lett.* **12**, 227.

Machetel, P. & Yuen, D. A. 1988 *Mathematical Geophysics*, (ed. N. J. Vlaar, G. Nolet, M. J. R. Wortel & S. A. P. L. Cloetingh), p. 265. D. Reidel.

Olson, P. 1987 *Phys. Earth Planet. Inter.* **36**, 337.
Olson, P. & Corcos, G. M. 1980 *Geophys. J. R. Astr. Soc.* **62**, 195.
Roberts, G. O. 1979 *Geophys. Astrophys. Fluid Dyn.* **12**, 235.
Robinson, J. L. 1967 *Intl J. Heat Mass Transfer* **12**, 1257.
Turcotte, D. L. & Oxburgh, E. R. 1967 *J. Fluid Mech.* **28**, 29.